UNIVERSITY OF SOUTHERN CALIFORNIA

DEPARTMENT OF CIVIL ENGINEERING

ANALYSIS OF A FEEDBACK TRANSDUCER

by

Ali Amini and Mihailo Trifunac

Report No. 83-03

A Report on Research Conducted under a Grant
from the National Science Foundation

Los Angeles, California

August 1983

TABLE OF CONTENTS

LIST OF FIGURES

LIST OF FIGURES (CONT.)

LIST OF TABLES

Introduction

Force-balance transducers (FBT) differ from other types of transducers in that they have an electrical feedback loop. An equilibrium state of the transducer mass is obtained by balancing the input force (caused by the absolute base acceleration) with an opposing force exerted on the mass proportional to the output voltage or current of a force generator. To approach equilibrium, an electrical pick-up (usually a capacitive type) is used to sense the relative mass movement, and its output is converted into the required feedback current or voltage to drive a force generator by way of an amplifier. The relative displacement sensor can be supplemented by a relative velocity-sensing device. This can be effected through an electro-dynamic generator type transducer in the feedback loop or by phase-shifting networks in the main loop.

Force-balance transducers can offer a wider useful frequency response range than the open-loop conventional transducers. Damping can be achieved through a phase-shifting network or by a velocity-sensing pick-up in the feedback loop. Both the damping and the natural frequency can be adjusted and altered by variation of the electrical components in the circuits of the feedback loop. It should be noted that mechanical stiffness and damping are often negligible compared with electrically produced equivalent terms, and can often be ignored in the equilibrium analysis of the transducer vibrating mass.

As pointed out by Neubert [4], instability due to environmental factors in the displacement and velocity sensors and in the amplifier does not affect the accuracy of the force-balance transducers. However instability in the force generator does, since the feedback current or voltage is taken as a measure of the input force. Thus, the problem of transducer stability has been

shifted from sensing element and amplifier to the force generator.

We begin by considering a typical block diagram of a force-balance accelerometer (Figure 1) and consider its input-output relations. Acceleration applied along the axial direction of the FBT causes a relative displacement of the mass which is sensed by a variable capacitance with sensitivity of D(V/m). Its output voltage is fed to an amplifier of gain K and a velocity-sensing pick-up such as an electrodynamic generator type transducer, or by phase-advancing network with a transfer function $(1 + \gamma \frac{d}{dt})$ thus providing the feedback damping. The output current i (Amp.) is fed to force generator with a factor of G(N/Amp), hence completing the loop by generating a force necessary to balance the input inertia force produced by acceleration.

Hudson [3] studied the system shown in Figure 1 and derived the following equations:

with
$$\ddot{X}_a = \ddot{X}_r + \ddot{X}_g \tag{1}$$

$$m\ddot{X}_r + (C + \frac{DKG\gamma}{R_o})\dot{X}_r + (K + \frac{DKG}{R_o})X_r = -m\ddot{X}_g \tag{2}$$

or
$$\ddot{X}_r + 2\omega_n \zeta \dot{X}_r + \omega_n^2 X_r = -\ddot{X}_g \tag{3}$$

where
$$2\omega_n\zeta = (\frac{C}{m} + \frac{DKG\gamma}{mR_o}) \tag{4}$$

$$\omega_n^2 = (\frac{K}{m} + \frac{DKG}{mR_o}) \tag{5}$$

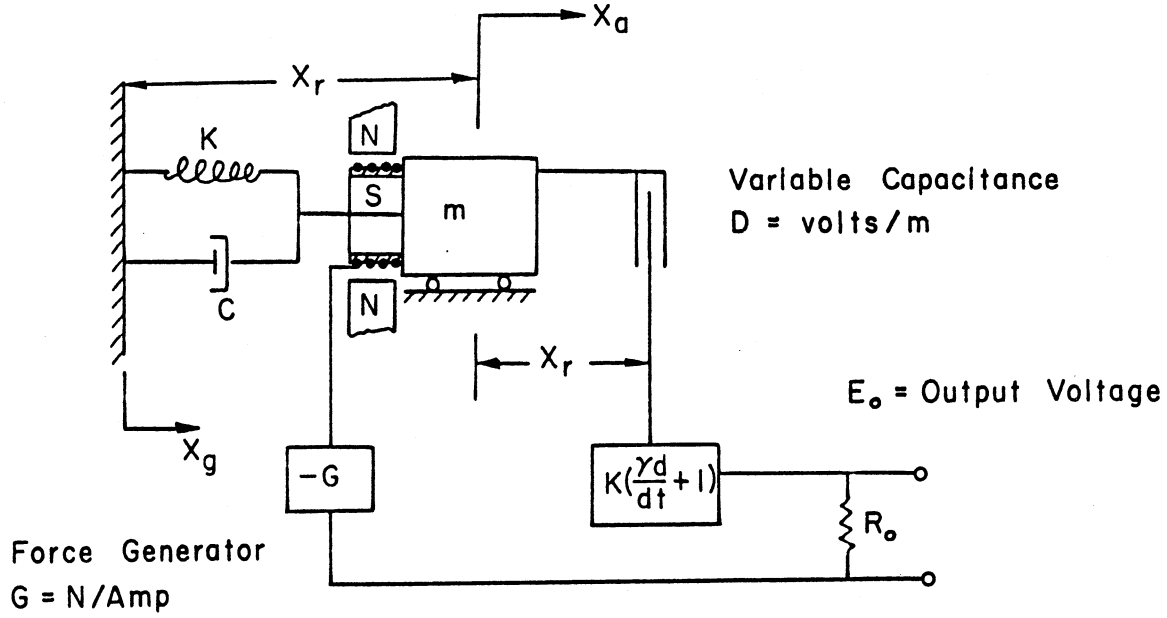

Figure 1. Force Balance Accelerometer Block Diagram

The balancing force on mass m and the output voltage are specified by:

$$\text{Balancing force on m} = -G\,\frac{E_o}{R_o} = -\frac{DKG}{R_o}X_r - \frac{DKG\gamma}{R_o}\dot{X}_r \tag{6}$$

$$\text{Output voltage: } E_o = DK(X_r + \gamma\dot{X}_r). \tag{7}$$

For a sinusoidal ground acceleration

$$\ddot{X}_g = a_g \sin\omega t$$

The instrument response then becomes:

$$E_o = \frac{DKa_g}{\omega_n^2}\,\frac{\sqrt{1+\gamma^2\omega^2}}{\sqrt{[1-(\frac{\omega}{\omega_n})^2]^2 + [2(\frac{\omega}{\omega_n})\zeta]^2}}\,\sin(\omega t - \phi) \tag{8}$$

Due to the fact that mechanical stiffness K and damping constant C are small compared to electrical stiffness $\frac{DKG}{R_o}$ and damping $\frac{DKG\gamma}{R_o}$, it follows from Equations (4) and (5) that Equation (8) can be written as

$$E_o = (\frac{mR_o}{G})\,a_g\,\frac{\sqrt{1+[2(\frac{\omega}{\omega_n})\zeta]^2}}{\sqrt{[1-(\frac{\omega}{\omega_n})^2]^2 + [2(\frac{\omega}{\omega_n})\zeta]^2}}\,\sin(\omega t - \phi) \tag{9}$$

For the sake of simplification, Equation (9) is written as follows:

$$E_o = (\frac{mR_o}{G})\,a_g A \sin(\omega t - \phi) \tag{10}$$

where

$$A = \frac{\sqrt{1 + [2(\frac{\omega}{\omega_n})\zeta]^2}}{\sqrt{[1 - (\frac{\omega}{\omega_n})^2]^2 + [2(\frac{\omega}{\omega_n})\zeta]^2}} \tag{11}$$

and the phase shift ϕ is specified by

$$-\phi = \tan^{-1} \frac{2(\frac{\omega}{\omega_n})^3}{1 + (\frac{\omega}{\omega_n})^2(4\zeta^2 - 1)} . \tag{12}$$

Comparison between the conventional tranducer and the FBT is considered by Hudson, and the result is shown in Figures 2 and 3. Figure 2 depicts the response amplitude A, while Figure 3 shows the graph of phase shift ϕ versus the ratio of forcing frequency to the natural frequency $(\frac{\omega}{\omega_n})$ for a fixed damping.

It is clear from the work of Hudson that the advantages of force-balanced transducers are: (1) the broadening of the frequency response range; (2) the possibility to alter natural frequency or damping of the transducer by changing the electrical constants in the feedback loop. It should be also noted that in the FBT considered by Hudon (Figure 1) the output voltage is proportional to relative displacement and velocity. However in many FBA's such as FBA-1 of Kinemetrics, Inc. the output voltage is proportional to relative displacement only. Therefore, the FBA-1 acts as a conventional transducer but with a higher natural freuquency.

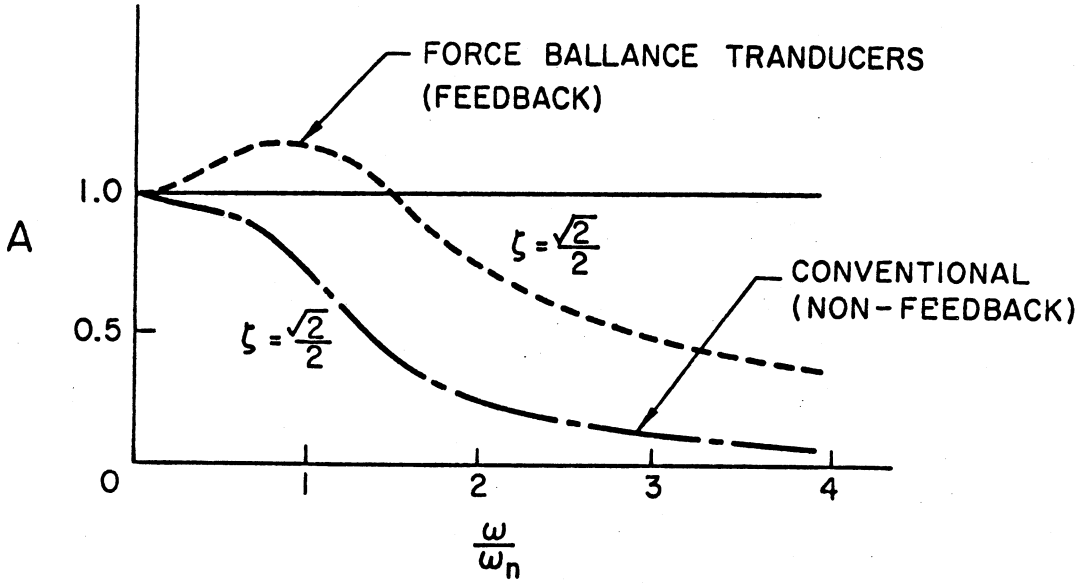

Figure 2. Response Amplitude (Normalized) as a Function of Frequency Ratio ω/ω_n

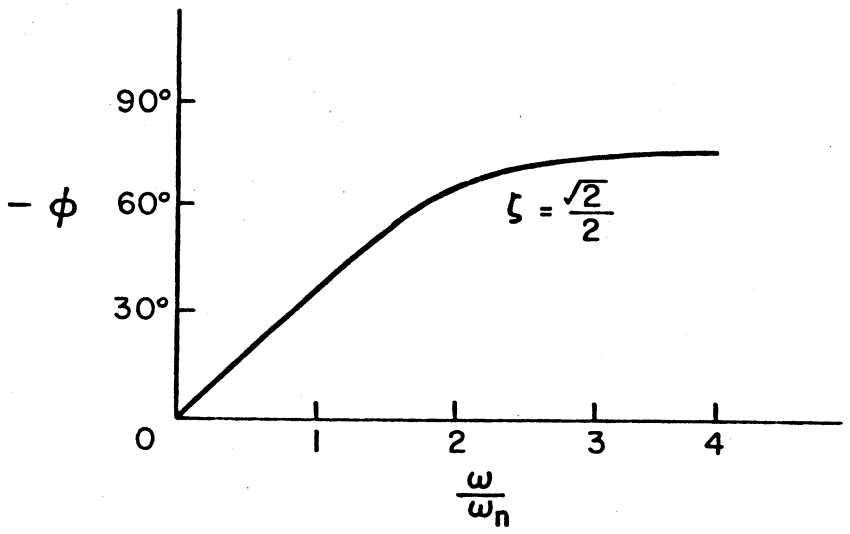

Figure 3. Response Phase Shift as a Function of ω/ω_n.

Statement of the Problem

The purpose of this paper is to refine and re-evaluate the differential equation (transfer function) of a typical force-balance accelerometer by considering all electrical components and filters that exist in such a system. Such a study consists of two parts: (1) theoretical evaluation of the transfer function of a typical force-balanced accelerometer, and (2) experimental verification of theoretical results. For doing such work, Kinemetrics, Inc., generously offered to us the use of one of their force-balanced accelerometers (FBA-1 #11749). We were also provided with the physical characteristics of the instrument, its circuit diagram (Figure 4), diagrams showing the locations of electrical components (Figure 5), Accelerometer Calibration Data Sheets (Figure 6), and other useful information pertaining to design and testing of the FBA-1. Kinemetrics also provided a PT06E-12-10S connector.

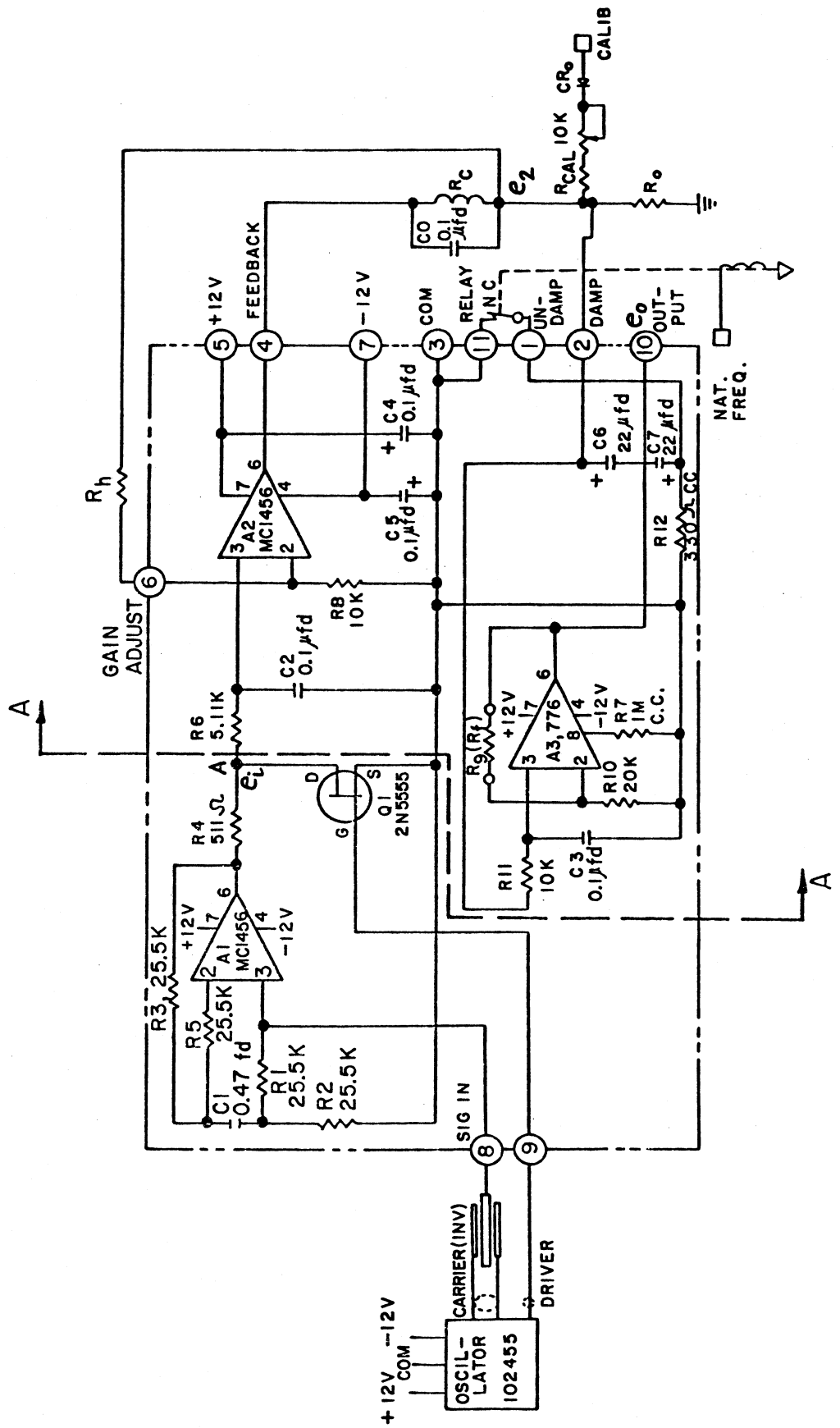

Figure 4. FBA-1 Circuit Diagram

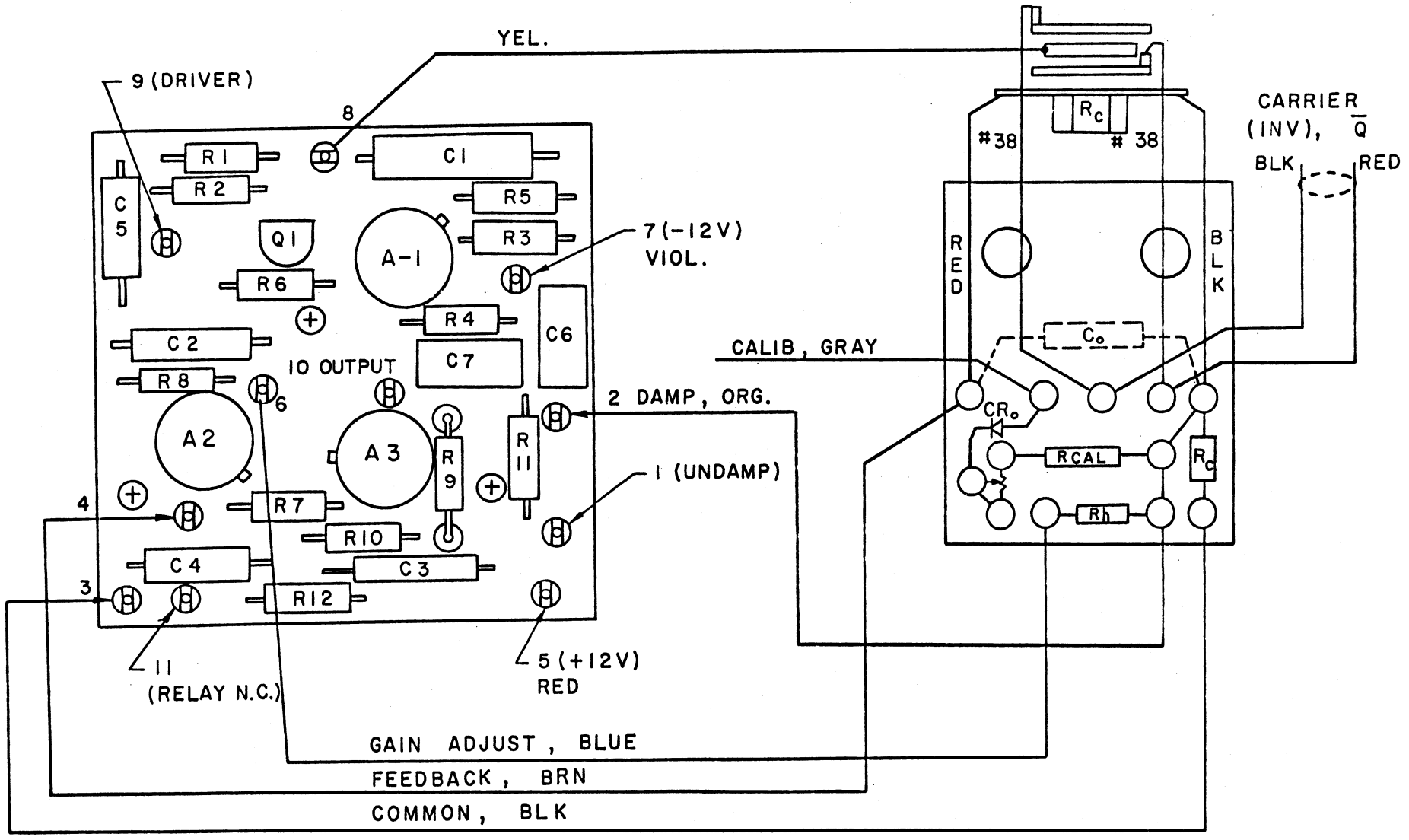

Figure 5. Electrical and Mechanical Component Location for FBA-1

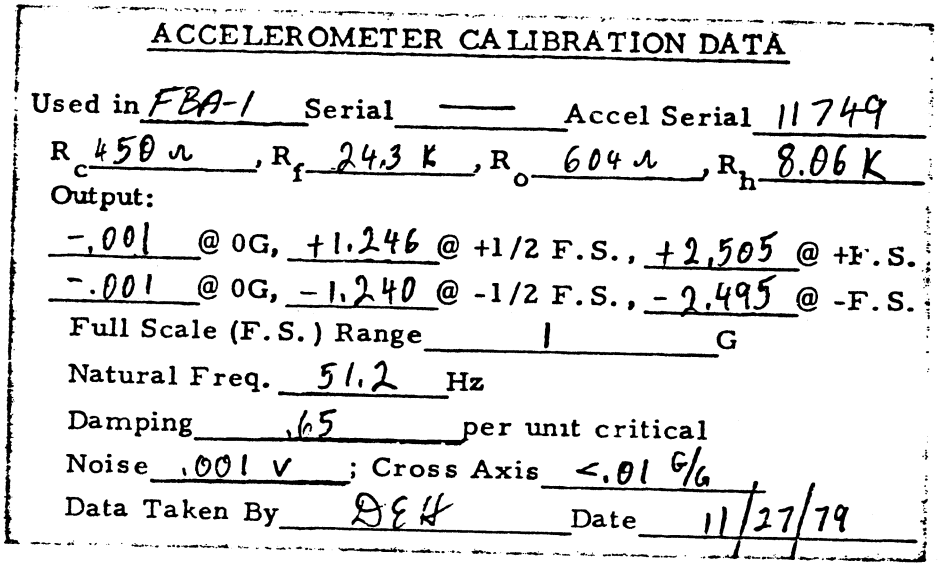

ACCELEROMETER CALIBRATION DATA

Used in FBA-1 Serial —— Accel Serial 11749

R_c 450 Ω, R_f 24.3 K, R_o 604 Ω, R_h 8.06 K

Output:

-.001 @ 0G, +1.246 @ +1/2 F.S., +2.505 @ +F.S.

-.001 @ 0G, -1.240 @ -1/2 F.S., -2.495 @ -F.S.

Full Scale (F.S.) Range 1 G

Natural Freq. 51.2 Hz

Damping .65 per unit critical

Noise .001 V ; Cross Axis <.01 G/G

Data Taken By DEH Date 11/27/79

Figure 6. FBA-1 Calibration Data

Theoretical Analysis

A block diagram of the FBA-1 is shown in Figure 7. Three important factors should be noted here: (1) the existence of the modulator and demodulator unit; (2) the portion that contributes to damping (the velocity sensing pickup, a differentiation element); and (3) force generator element and its current I_1.

Since the position sensing in this type of instrument is done by a variable capacitor which does not respond to D.C., a carrier and driver are needed for the purpose of modulation and demodulation of the input voltage $DX_r(\frac{V}{m} \cdot m)$. Modulation and demodulation do not affect the transfer function of the system, so they can be ignored in the derivation.

In a typical force-balance accelerometer, the velocity-sensing pick-up is either the phase-shifting network (differentiator) in the main loop [4] or an electrodynamic generator type transducer in the feedback loop [4].

From experimental and theoretical analysis, it follows that the velocity-sensing pick-up used for damping in the Kinemetrics FBA-1 is a combination of the electrical components and the voltage induced in the coil in the feedback loop of the circuit.

With reference to Figures 4 and 7, it is of importance to note that the current which flows through R_c and L_c is the current that balances the force on mass M through the force generator G(N/Amp).

To evaluate the transfer function of the FBA-1, Figure 7 has been divided into four parts. The transfer function of each part is evaluated separately and then the total transfer function is derived by combining the separate results.

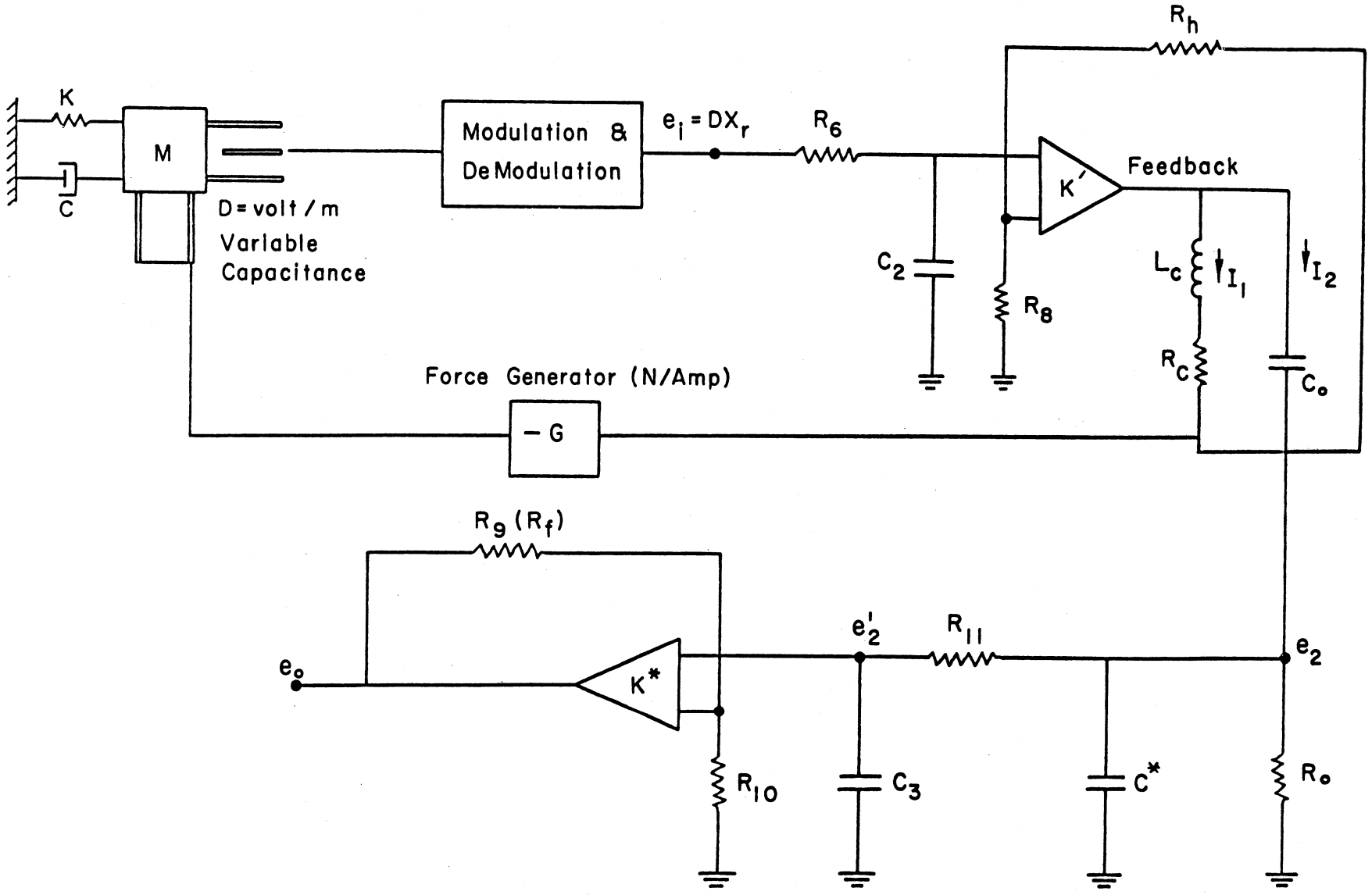

Figure 7. Forced Balance Accelerometer (FBA-1) Schematic Diagram.

Part 1

The input into this part is $e_i = DX_r$ volts. It represents a low-pass filter with corner frequency of about 310 Hz. Its main purpose is to eliminate the high frequencies introduced into the system by the modulation part. For all practical purposes, this part may be ignored due to its high corner frequency; however, for the sake of completeness, it is included in the analysis of the transfer function of the force-balanced accelerometer (FBA). The circuit diagram of this stage is shown in Figure 8.

The transfer function of part 1 can be written as:

$$\frac{e_i'}{e_i} = \frac{e_i'}{DX_r} = \frac{1}{1 + R_6C_2S} \tag{13}$$

or in terms of frequency

$$\frac{e_i'}{e_i} = \frac{e_i'}{DX_r} = \frac{1}{1 + j\omega R_6C_2} \tag{14}$$

Part 2

The input into Part 2 is the output of Part 1 (Figure 7). This part is the most important one of the FBA-1. It has an amplifier and feeds back the signal to balance forces on the mass M. The damping and natural frequency are also controlled by this stage.

The circuit diagram of Part 2 is shown in Figure 9. The capacitor C* has a value of about 11 μf which is the combination of C_6 and C_7 as shown in Figure 4. The value of R_c is about 450 ohms. The inductance of the coil is indicated by L_c. The voltage produced in the coil is given by:

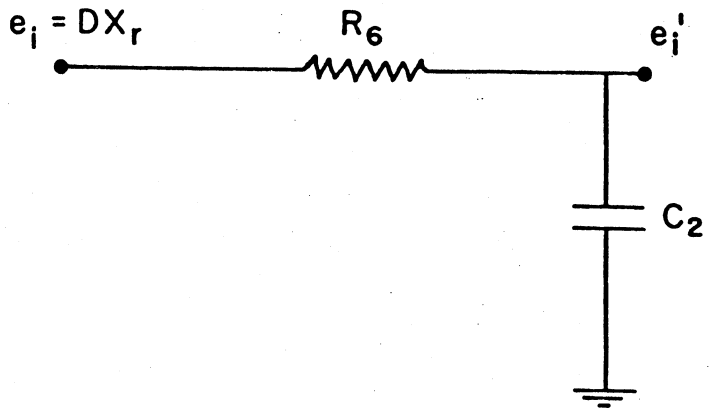

Figure 8. Part 1 Circuit Diagram

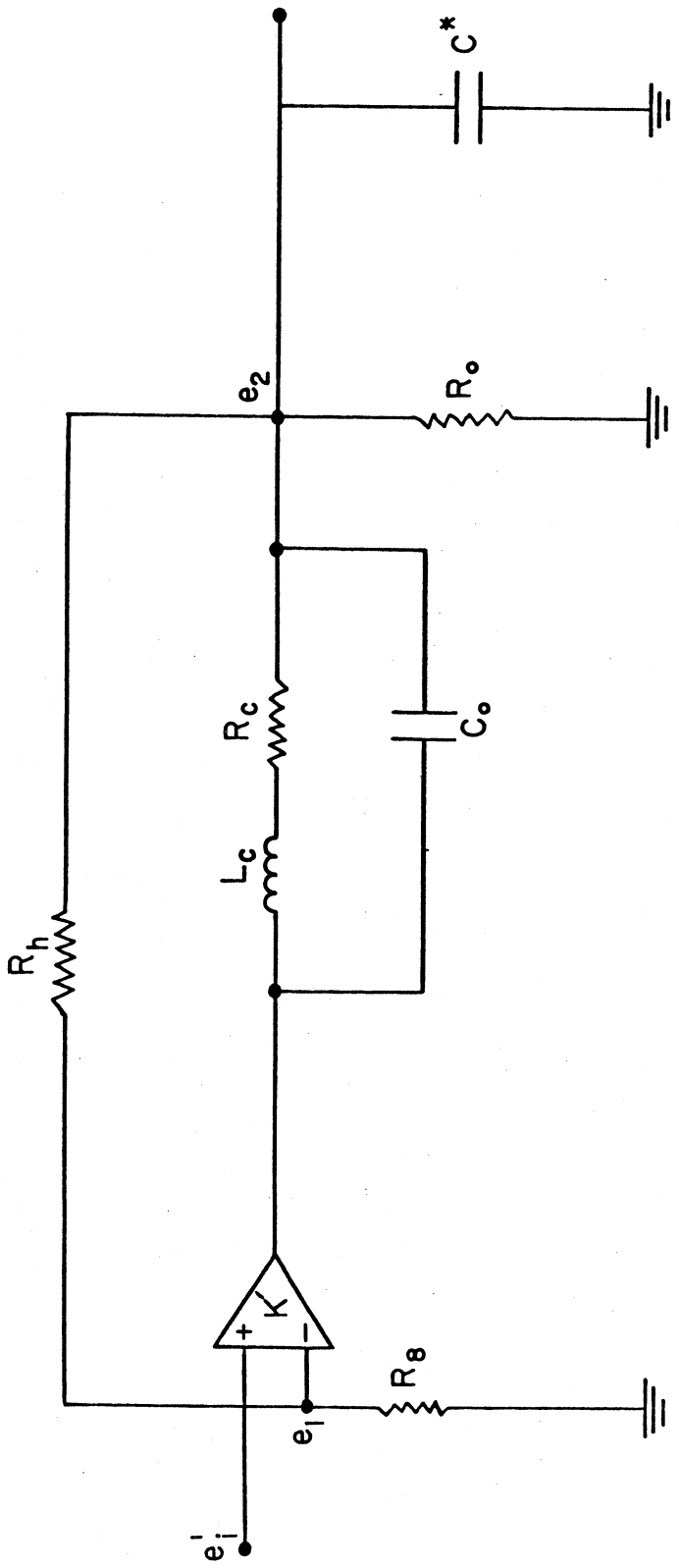

Figure 9. Part 2 Circuit Diagram.

$$E_c = I_1(R_c + SL_c) \tag{15}$$

To analyze Part 2, we introduce its equivalent circuit diagram (Figure 10).

It follows from Figure 10 that

$$e_1 = \frac{R_8}{R_8 + R_h} e_2 \tag{16}$$

For the sake of simplification, we define the following notation:

$$R = (R_o)||(R_h + R_8) = \frac{R_o(R_h + R_8)}{R_o + R_h + R_8} \tag{17}$$

$$R^* = R||\frac{1}{SC^*} = \frac{R}{1 + RC^*S} \tag{18}$$

With this in mind, the equivalent circuit of stage 2 can be redrawn as shown in Figure 11.

By considering the current law at the common node, it follows that

$$[K'(e_i' - e_1) - e_2]\, SC_o + \frac{K'(e_i' - e_1) - e_2}{R_c + SL_c} = \frac{e_2}{R^*} \tag{19}$$

Substitution of equation (16) into equation (19) implies

$$SC_oK' - \frac{e_2}{e_i'}\left(\frac{K'R_8SC_o}{R_h + R_8} + SC_o\right) + \frac{K'}{R_c + SL_c}$$

$$- \frac{e_2}{e_i'}\left[\frac{K'R_8}{(R_8 + R_h)(R_c + SL_c)} + \frac{R^* + R_c + SL_c}{R^*(R_c + SL_c)}\right] = 0 \tag{20}$$

which can be written in the following form:

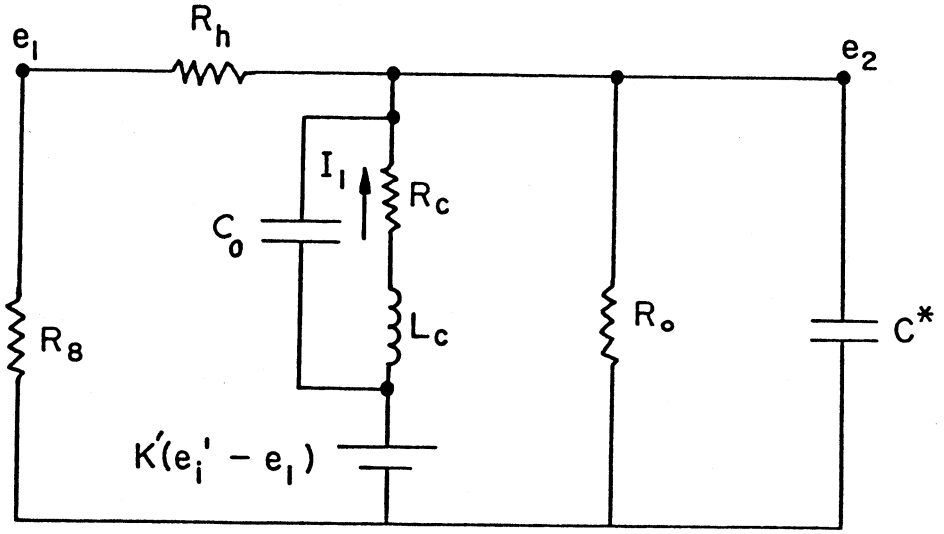

Figure 10. Part 2 Equivalent Circuit Diagram

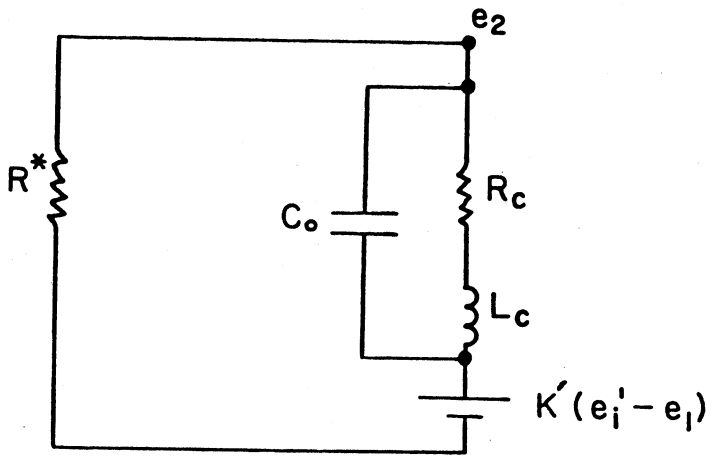

Figure 11. Part 2 Equivalent Circuit Diagram

$$\frac{e_2}{e_i'} = \frac{K'R^*[(R_c + SL_c)SC_o + 1](R_h + R_8)}{\{K'R_8R^*[(R_c + SL_c)SC_o + 1] + SC_oR^*(R_h + R_8)(R_c + SL_c) + (R^* + R_c + SL_c)(R_h + R_8)\}} \tag{21}$$

Equation (21) gives the exact transfer function between nodes e_i' and e_2. (See Figure 11.) Since a typical value of K' is about 100 K (MC1456), the second portion of the denominator of Equation (21) is usually ignored. Therefore, we have

$$\frac{e_2}{e_i'} \cong \frac{(R_h + R_8)}{R_8} \tag{22}$$

It appears from Equations (22) and (16) that the values of e_1 and e_i' are the same, but remember that Equation (22) is approximate. The difference between the two voltages is of the order of 10^{-5} v, and this difference produces voltage $K'(e_i' - e_1)$. Equation (22) indicates that there is no phase-shifting between the nodes e_2 and e_i', only an amplification of $\frac{R_h + R_8}{R_8} = 1.8$.

To find where the electrical damping and natural frequency come from, we need to evaluate the current I_1 (Figure 10) which is the important factor in balancing the forces on mass M. From Equation (19), the value of $K'(e_i' - e_1)$ can be written as

$$K'(e_i' - e_1) = \frac{e_2[R_c + R^* + SL_c + R^*(R_c + SL_c)SC_o]}{R^*[1 + SC_o(R_c + SL_c)]} \tag{23}$$

The current I_1 (see Figure 10) is given by

$$I_1 = \frac{K(e_i' - e_1) - e_2}{R_c + SL_c} \tag{24}$$

Substituting Equation (23) into Equation (24) results in

$$I_1 = \frac{e_2}{R^*[1 + SC_o(R_c + SL_c)]} \tag{25}$$

Substituting the value of R* from Equation (18) in Equation (25) gives

$$I_1 = \frac{e_2(1 + RC^*S)}{R[1 + SC_o(R_c + SL_c)]}$$

By use of Equations (22) and (13), I_1 can be written as

$$I_1 = \frac{(\frac{R_h + R_8}{R_8})(\frac{1}{1 + R_6C_2S})(1 + RC^*S)e_i}{R[1 + SC_o(R_c + SL_c)]} \tag{27}$$

The values of C_2 and C_o are small, however, to observe their contributions to the natural frequency and the damping of the complete system these capacitors are not neglected. Substituting the value of R from Equation (17) into Equation (27), there follows:

$$I_1 = \frac{(\frac{R_o + R_h + R_8}{R_oR_8} + \frac{R_h + R_8}{R_8} C^*S)e_i}{[1 + SC_o(R_c + SL_c)](1 + R_6C_2S)} \tag{28}$$

Note that $e_i = DX_r$ volts. It is clear from Equation (28) that if we had ignored the denominator due to low values of C_o and C_2, the first term of numerator would be the main contributor to the natural frequency while the second term would contribute to the damping. This point becomes more obvious when we write the equilibrium equation of the mass-spring system with feedback. The S domain is kept throughout the forthcoming analysis, since the

electrical components are already in that form. However, at the end of the presentation we also consider the time domain, as a form of comparison with the results of Hudson [3]. With this in mind, we can write the equilibrium equation of the mass-spring system (Figure 7).

$$MS^2X_r = -KX_r - CSX_r - GI_1 - MA(S) \tag{29}$$

where A(S) is the acceleration in S domain.

Substituting Equation (28) into the Equation (29) and neglecting the small coefficients of the third and the fourth power of S, there follows:

$$\frac{X_r}{-A(S)} = \frac{A^*}{S^2 + 2\zeta\omega_n S + \omega_n^2} \tag{30}$$

where

$$A^* = \frac{M}{M + KC_oL_c + KC_oR_cC_2R_6 + CC_oR_c + CC_2R_6}, \tag{31}$$

$$2\zeta\omega_n = \frac{C + KC_oR_c + KC_2R_6 + GDC^* \dfrac{(R_h + R_8)}{R_8}}{M + KC_oL_c + KC_oR_cC_2R_6 + CC_oR_c + CC_2R_6}, \tag{32}$$

$$\omega_n^2 = \frac{K + GD \dfrac{R_o + R_h + R_8}{R_oR_8}}{M + KC_oL_c + KC_oR_cC_2R_6 + CC_oR_c + CC_2R_6}, \tag{33}$$

Next, one can consider a simple form of Equation (28) as

$$I_1 \simeq \left(\frac{R_o + R_h + R_8}{R_oR_8} + \frac{R_h + R_8}{R_8} C^*S\right)e_i \ . \tag{34}$$

If we follow the same procedure as before the parameters of Equations (30) can be written as:

$$A^* \simeq 1 \ , \tag{35}$$

$$2\zeta\omega_n \simeq \frac{C}{M} + \frac{DGC^*}{M}\frac{R_h + R_8}{R_8} \tag{36}$$

$$\omega_n^2 \simeq \frac{K}{M} + \frac{DG}{M}\frac{R_o + R_h + R_8}{R_o R_8} \tag{37}$$

In general the spring constant K and the damping C are small compared to their corresponding electrical quantities. Hence Equations (36) and (37) reduce to

$$2\zeta\omega_n \simeq \frac{DGC^*}{M}\frac{R_h + R_8}{R_8} \ , \tag{38}$$

$$\omega_n^2 \simeq \frac{DG}{M}\frac{R_o + R_h + R_8}{R_o R_8} \tag{39}$$

Since the measured output is not X_r but e_o (see Figure 7), there are still two more stages to be considered.

Part 3

The input for this part is the output of stage 2, which is denoted by e_2. This stage, as shown in Figure 12, is another low pass filter with corner frequency of about 160 Hz. Its main purpose is to eliminate any high-frequency modulation contributions not eliminated in Stage 1. Since the frequencies of interest are smaller than 160 Hz, the effects of

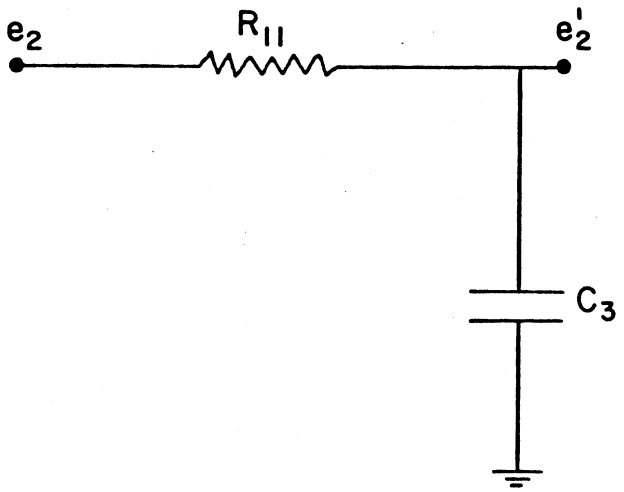

Figure 12. Part 3 Circuit Diagram

this stage, similar to stage 1, can be ignored in calculations. However, for the completeness of the theory, this stage is also included.

The transfer function of this part can be written as:

$$\frac{e_2'}{e_2} = \frac{1}{1 + R_{11}C_3S} \tag{40}$$

or in terms of frequency

$$\frac{e_2'}{e_2} = \frac{1}{1 + j\omega R_{11}C_3} \tag{41}$$

Part 4

This segment, which is the last stage of the FBA-1 logic, is a post-amplification part. Its input is the output of stage 3, that is, e_2', and its output is e_o which is usually connected to a recording station. The circuit diagram of this part is shown in Figure 13. To analyze this stage, consider its equivalent circuit diagram shown in Figure 14. For the circuit of Figure 14, the following equations hold:

$$e_1' = \frac{R_{10}}{R_{10} + R_9} e_o \tag{42}$$

and

$$\frac{K*(e_2' - e_1')}{R_{10} + R_9} = \frac{e_o - e_1'}{R_9} \tag{43}$$

Substituting e_1' from Equation (42) into Equation (43) results in

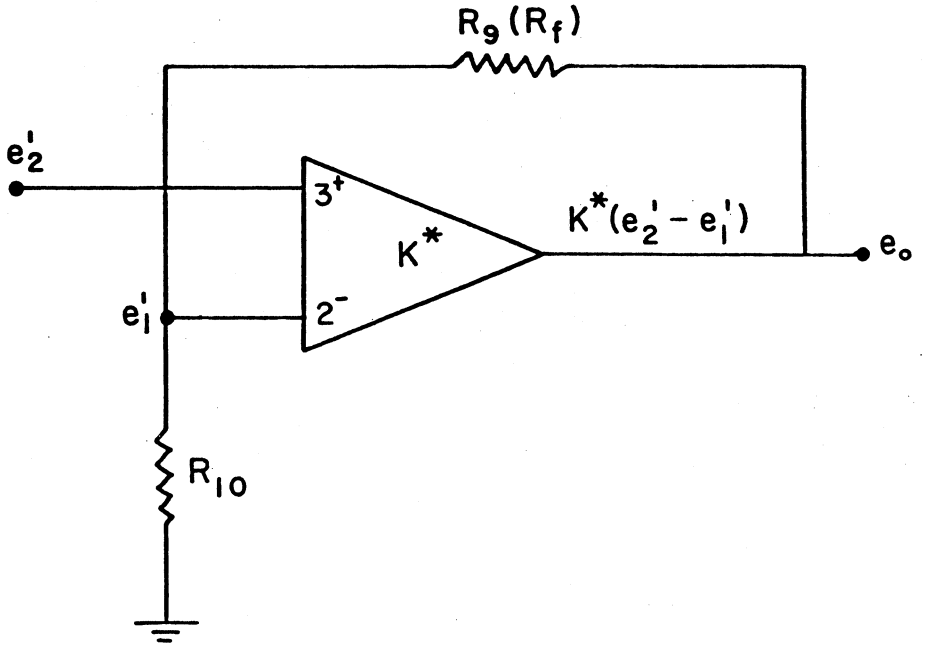

Figure 13. Part 4 Circuit Diagram

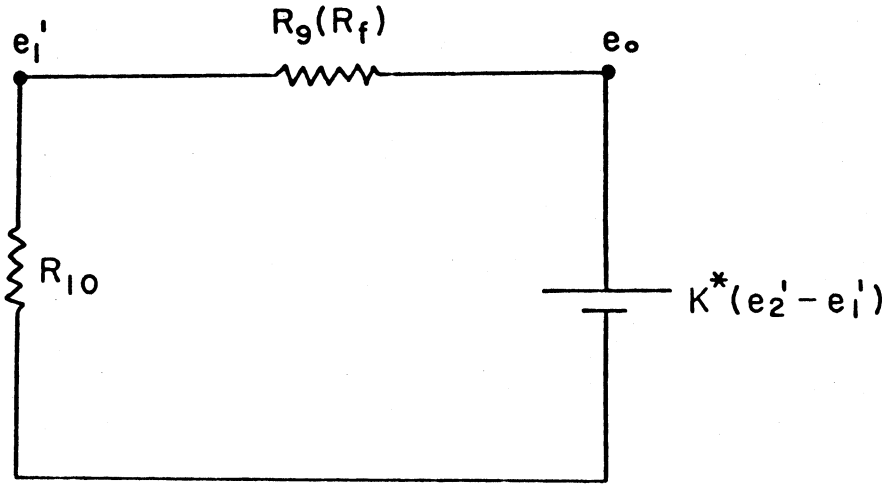

Figure 14. Part 4 Equivalent Circuit Diagram

$$\frac{e_o}{e_2'} = \frac{K^*(R_{10} + R_9)}{K^*R_{10} + (R_{10} + R_9)} \tag{44}$$

Since the value of K* is very large, Equation (44) can be written approi-mately as

$$\frac{e_o}{e_2'} \cong \frac{R_{10} + R_9}{R_{10}} \tag{45}$$

As it may be clear from Equation (45), the part 4 is an amplifier, with amplification value of about $\frac{R_{10} + R_9}{R_{10}} = 2.22$.

Complete Transfer Function

Now that the transfer function of each part is known, we can derive the complete transfer function of the FBA-1 accelerometer. Using the fact that $e_i = DX_r$, along with Equations (45), (40), (22), and (13), the output voltage e_o can be written as

$$e_o = \frac{R_{10} + R_9}{R_{10}} \cdot \frac{1}{1 + R_{11}C_3S} \cdot \frac{R_h + R_8}{R_8} \cdot \frac{1}{1 + R_6C_2S} \cdot DX_r \tag{46}$$

Substituting the value of X_r from Equation (30) gives

$$\boxed{e_o = \frac{R_{10} + R_9}{R_{10}} \cdot \frac{R_h + R_8}{R_8} \cdot \frac{1}{1 + R_{11}C_3S} \cdot \frac{1}{1 + R_6C_2S} \cdot \frac{-DA(S) \cdot A^*}{S^2 + 2\omega_n\zeta S + \omega_n^2}} \tag{47}$$

where A*, $2\zeta\omega_n$ and ω_n^2 are defined by Equations (31), (32) and (33) respec-tively. Equation (47) is the complete transfer function of the system.

As can be seen, both low pass filters are included in this equation. An approximate form of Equation (47) may be written as

$$e_o = D \frac{R_{10} + R_9}{R_{10}} \quad \frac{R_h + R_8}{R_8} \quad \frac{-A(s)}{S^2 + 2\omega_n \zeta S + \omega_n^2} \tag{48}$$

The damping, ζ, and natural frequency, ω_n, are defined by Equations (38) and (39), and the value of $A^* = 1$.

At this point, it is interesting to compare the above results with those of Hudson. We consider Equation (29) in the time domain, with I_1 represented by Equation (34) and $2\zeta\omega_n$ and ω_n^2 represented by Equations (38) and (39) respectively. It follows from the equilibrium considerations of mass M that,

$$M\ddot{X}_r \simeq - GD \frac{R_o + R_h + R_8}{R_o R_8} X_r - GD \frac{R_h + R_8}{R_8} C^* \dot{X}_r - M\ddot{X}_g \tag{49}$$

or

$$\ddot{X}_r + \frac{GD}{M} \cdot \frac{R_h + R_8}{R_8} C^* \dot{X}_r + \frac{GD}{M} \frac{R_o + R_h + R_8}{R_o R_8} X_r \simeq -\ddot{X}_g \tag{50}$$

Through use of Equations (38) and (39), the last result becomes

$$\ddot{X}_r + 2\zeta\omega_n \dot{X}_r + \omega_n^2 X_r \simeq - \ddot{X}_g \tag{51}$$

For a sinusoidal ground acceleration

$$\ddot{X}_g = a_g \sin\omega t, \tag{52}$$

The relative displacement X_r is given by

$$X_r \simeq \frac{a_g \rho}{\omega_n^2} \sin(\omega t - \theta) \tag{53}$$

where

$$\rho = \frac{1}{\sqrt{[1 - (\frac{\omega}{\omega_n})^2]^2 + [2(\frac{\omega}{\omega_n})\zeta]^2}} \tag{54}$$

$$\theta = \tan^{-1} \frac{2\zeta\frac{\omega}{\omega_n}}{1 - (\frac{\omega}{\omega_n})^2} \tag{55}$$

As noted earlier, DX_r is the input to Part 1. Considering the amplifications present in the system, the output voltage e_o is given by

$$e_o \simeq \frac{R_{10} + R_9}{R_{10}} \quad \frac{R_h + R_8}{R_8} \quad \frac{D\, a_g}{\omega_n^2} \rho \sin(\omega t - \theta) \tag{56}$$

The key parameters in Equation (56) are ρ and θ, compared to Hudson's A and ϕ [see Equations (11) and (12)]. Graphs of ρ and θ are shown in Figures 15 and 16, respectively, for the damping of $\sqrt{2}/2$.

The basic difference between the above results and those of Hudson should be clear by comparing Equations (54) and (55) with Equations (11) and (12). The difference in the two results is due to the fact that in the present analysis, the output voltage is proportional to relative displacement only, and the 90° phase shift produces electrical damping, while the velocity $\dot{X}_r$ itself is not part of the output [see Equation (56)]. Hence, the system acts as a single-degree-of-freedom system which rolls off at

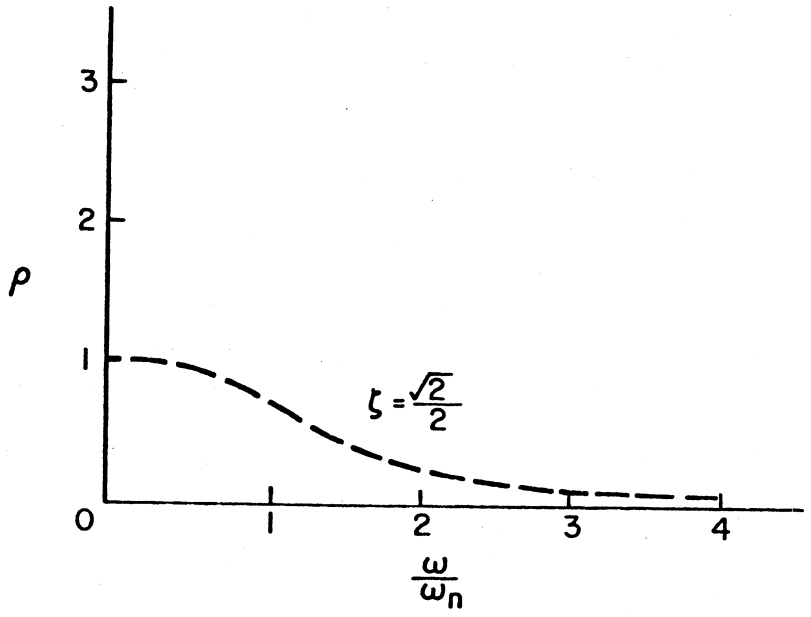

Figure 15. Response Amplitude (Normalized) as a Function of ω/ω_n for the FBA-1 (Filters Not Included).

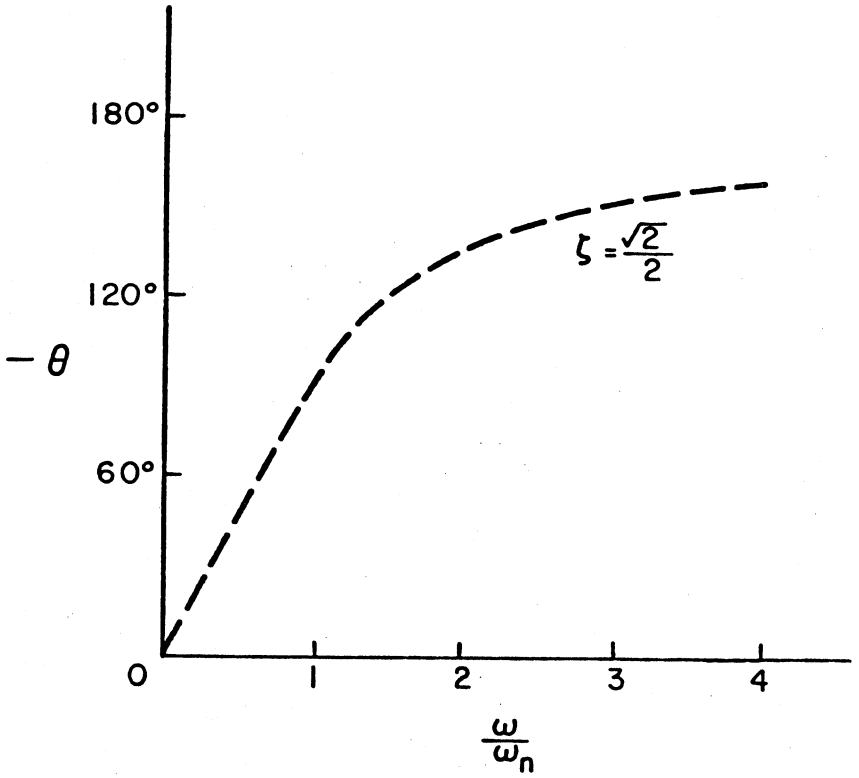

Figure 16. Response Phase Shift as a Function of ω/ω_n for FBA-1 (Filters Not Included).

its corner frequency as shown in Figure 15. The output voltage in Hudson's model is proportional to relative displacement X_r and relative velocity $\dot{X}_r$ [see Equation (7)], thus producing response which first increases and then rolls off, as seen in Figure 2. It should be clear that in this comparison the contributions of the filters and capacitor C_o are neglected. Thus it appears that Kinemetrics FBA-1 acts much like a conventional transducer but with a higher corner frequency due to the feedback loop.

Experiments

The experimental work on the force-balance accelerometer (FBA-1 #11749) has been devided into three tasks:

1. Measurement of damping and natural frequency of the FBA-1 following the procedure outlined in the Kinemetrics Operating Instructions for FBA-1, Force Balance Accelerometer, Part Number 102475.

2. Determination of electrical component transfer function. The mechanical mass and spring portion were isolated by disconnecting the circuit after modulation, at the resistor R_6, and a low-amplitude, low-frequency input voltage at that point was applied (see section A-A of Figure 4). By doing this, the effect of feedback is eliminated. This task was done to verify the gains of amplifiers (Parts 2 and 4) and the filtering of the two low-pass filters (Parts 1 and 3).

3. This task consisted of a shaking table test, producing the transfer function of the system as a whole. The testing performed in this task is based on comparison of the FBA-1 with another transducer having very high corner frequency. Both the FBA-1 and the reference transducer are subjected to the same random and sinusoidal wave excitation of the same shaking table. Thus, it is important that the reference transducer and the shaking table be of high quality and accuracy.

Task One

As mentioned previously, this task deals with evaluation of damping and natural frequency based on Kinemetrics operating instructions. For this test, the required +12 vdc and -12 vdc were supplied by Tektronix PS 503A power supply. Accelerometer zero adjustment was done through the use of Tektronix digital multimeter DM 501. The power supply and multimeter, along with a function generator, are all one packaged instrument, known as TM 503. Also, a rotary switch and chart recorder are used in this test.

Following Kinemetrics instructions with the speed of the chart recorder set at 125 mm/sec, the record was obtained as shown in Figure 17. From this record, the damping and natural frequency were evaluated. To calculate the damping, the overshoot ratio was computed. The overshoot ratio is $\frac{X_2}{X_1}$ (see Figure 17). Using this ratio, the damping can be evaluated by using Table 1, which was supplied by Kinemetrics.

For measuring the natural frequency, the number of cycles between two peak points were read, along with the distance between them (see Figure 17). By the exact speed of the chart recorder, the natural frequency is calculated to be 49.73 Hz. Note that the decay in sinusoid is due to mostly mechanical damping. This damping has a value of about 0.01, which supports the assumption that it might be eliminated from Equation (36).

It should be pointed out that at Kinemetrics, Inc., a different procedure for measuring damping and natural frequency is being used. By inserting 5 volts p-p at the CALIB input (see right-hand side of Figure 4) and by increasing the frequency from 2 Hz to 50 Hz, a check is made to note if output starts to decay as 50 Hz is approached. The output should decrease so that at 50 Hz it should be about 70% of the output at 2 Hz. If this is

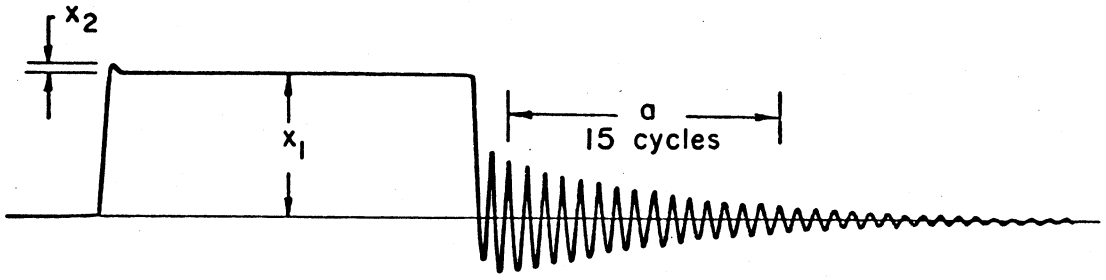

Overshoot ratio = $E = \frac{x_2}{x_1} = 0.06$

a = 37.7 mm

$E = 0.06 \longrightarrow \zeta = 0.67$ (Table 1)

$f_n = \frac{(125 \text{ mm/sec})\ 15 \text{ cycles}}{(37.7 \text{ mm})} = 49.73 \text{ Hz}$

Figure 17. Test Results for Measurements of Damping and Natural Frequency Based on Kinemetrics Operational Manual.

TABLE 1

OVERSHOOT RATIO VERSUS DAMPING

Damping h	Overshoot O.S.	Ratio
0.60	0.95	10.55/1
0.61	0.089	11.23/1
0.62	0.083	11.97/1
0.63	0.078	12.79/1
0.64	0.073	13.69/1
0.65	0.068	14.69/1
0.66	0.063	15.80/1
0.67	0.059	17.04/1
0.68	0.054	18.42/1
0.69	0.050	19.98/1
0.70	0.046	21.74/1
0.71	0.042	23.75/1
0.72	0.038	26.03/1
0.73	0.035	28.66/1
0.74	0.031	31.70/1
0.75	0.028	35.24/1
0.76	0.025	39.40/1
0.77	0.022	44.31/1
0.78	0.020	50.19/1
0.79	0.017	57.28/1
0.80	0.015	65.94/1

not so, R_o and R_h are simultaneously adjusted to get the desired values of natural frequency and damping, respectively. Kinemetrics values evaluated for damping and natural frequency, based on their procedure for the FBA-1 #11749, are 0.65 and 51.2 Hz, respectively, as seen in Figure 6.

Task 2

As discussed earlier, only a portion of the circuit shown in Figure 4 was used in this task. This is section A-A disconnected from the rest of the circuits (see Figure 4). It can be seen that this part is free of mechanical components. Therefore, Task 2 consists of a simple check of amplifications and filtering that exist in the circuit.

A low-amplitude sinusoidal input e_i at point "A" produces gain and phase shift at points e_2 and e_o (see Figure 4). Due to a limited accuracy of the testing instruments used in this experiment, the range of applied frequencies was only from 20 Hz to 200 Hz. Although lower frequencies were more desirable, the range of frequencies used was sufficient to satisfy the objective of Task 2. Measuring devices and instruments used in this part were: Tektronix oscilloscope 465, Serial No. B 325812; Tektronix TM 503, which includes a function generator, power supply, and digital multimeter. Also, a 24 K potentiometer was used to reduce the amplitude of the input voltage at point A of Figure 4.

Before stating the experimental results, the theoretical values are evaluated. Combining Equations (14) and (22) results in

$$\frac{e_2}{e_i} = \frac{R_h+R_8}{R_8} \frac{1}{1+j2\pi f\, R_6C_2} \tag{57}$$

Multiplying Equation (57) by Equations (41) and (45) results in

$$\frac{e_o}{e_i} = \frac{R_h + R_8}{R_8} \cdot \frac{R_{10} + R_9}{R_{10}} \cdot \frac{1}{1 + j2\pi f R_6 C_2} \cdot \frac{1}{1 + j2\pi f\, R_{11} C_3} \qquad (58)$$

Using the values of resistors and capacitors (see Figures 4 and 6) provided by Kinemetrics, the gain and the phase shift associated with Equations (57) and (58) can be evaluated. Table 2 shows the gain and phase-shift of $\frac{e_2}{e_i}$ as a function of frequency. Table 3 shows similar results for $\frac{e_o}{e_i}$. Figures 18 and 19 display theoretical gain and phase-shift of $\frac{e_2}{e_i}$, respectively, and Figures 20 and 21 show similar results for $\frac{e_o}{e_i}$.

The experimental results are shown in Tables 4 and 5. The plots of gain and phase-shift of $\frac{e_2}{e_i}$ and $\frac{e_o}{e_i}$ are shown in Figures 18, 19, 20, and 21, respectively, along with their theoretical values as discussed earlier. These figures indicate a good agreement between theoretical and experimental values of $\frac{e_2}{e_i}$ and $\frac{e_o}{e_i}$ (gain and phase shift). Small differences that exist are due to errors of the electrical constants of resistors and capacitors, and also due to errors involved in reading the gain and phase-shift from the oscilloscope. As mentioned earlier, this part excludes the mechanical portion and the feedback portion of the force-balanced accelerometer. However, it serves as a check of theoretical calculations.

There are some important facts that the above figures point out, especially Figures 20 and 21. Both the theoretical and experimental results of $\frac{e_o}{e_i}$ show a gain drop of about 50% from zero to 200 Hz and appreciable phase shifting.

Recall that in Equation (34) in calculating approximate value of the current through the coil, the effect of the first filter and C_o were neglected. Also in Equation (48) or similarly in Equation (49), the effects

TABLE 2

Theoretical Gain and Phase-Shift of $\frac{e_2}{e_i}$

as a Function of Frequency
(see Equation 57)

f(Hz)	$\left\|\frac{e_2}{e_i}\right\|$	Phase Shift, ^{o}
0	1.80	0
20	1.80	-3.67
30	1.79	-5.50
40	1.78	-7.32
50	1.78	-9.12
60	1.77	-10.90
70	1.76	-12.70
80	1.74	-14.40
90	1.73	-16.10
100	1.71	-17.80
110	1.70	-19.40
120	1.68	-21.10
130	1.66	-22.70
140	1.64	-24.20
150	1.62	-25.70
160	1.60	-27.20
170	1.58	-28.60
180	1.56	-30.00
190	1.54	-31.40
200	1.51	-32.70

TABLE 3

Theoretical Gain and Phase-Shift of $\frac{e_o}{e_i}$ (output)

as a Function of Frequency
(see Equation 58)

f(Hz)	$\lvert\frac{e_o}{e_i}\rvert$	Phase Shift, ^{o}
0	4.00	0
20	3.96	-10.83
30	3.90	-16.16
40	3.83	-21.40
50	3.77	-26.60
60	3.68	-31.50
70	3.57	-36.40
80	3.45	-41.10
90	3.34	-45.60
100	3.21	-49.90
110	3.10	-54.00
120	2.97	-58.10
130	2.85	-61.90
140	2.73	-65.50
150	2.62	-69.00
160	2.50	-72.30
170	2.39	-75.50
180	2.29	-78.50
190	2.19	-81.40
200	2.09	-84.00

TABLE 4

Experimental Gain and Phase-Shift of $\frac{e_2}{e_i}$

as a Function of Frequency

f(Hz)	$\lvert\frac{e_2}{e_i}\rvert$	Phase Shift, ^{o}
20	1.80	-3.00
30	1.75	-9.00
40	1.75	-9.90
50	1.72	-11.25
60	1.70	-13.50
70	1.70	-16.65
80	1.70	-18.00
90	1.67	-18.00
100	1.65	-18.00
110	1.65	-19.90
120	1.65	-20.00
130	1.62	-23.90
140	1.62	-25.60
150	1.60	-27.00
160	1.60	-27.00
170	1.52	-30.00
180	1.51	-31.00
190	1.46	-31.00
200	1.42	-36.00

TABLE 5

Experimental Gain and Phase-Shift of $\frac{e_o}{e_i}$

as a Function of Frequency

f(Hz)	$\lvert\frac{e_o}{e_i}\rvert$	Phase Shift, ^{o}
20	3.90	-9.26
30	3.80	-18.00
40	3.80	-21.00
50	3.70	-24.00
60	3.60	-30.00
70	3.50	-36.00
80	3.35	-40.50
90	3.20	-45.90
100	3.15	-49.50
110	3.10	-54.00
120	2.90	-58.50
130	2.65	-63.00
140	2.65	-65.25
150	2.50	-69.75
160	2.40	-72.00
170	2.35	-72.00
180	2.25	-76.50
190	2.12	-81.00
200	2.00	-81.00

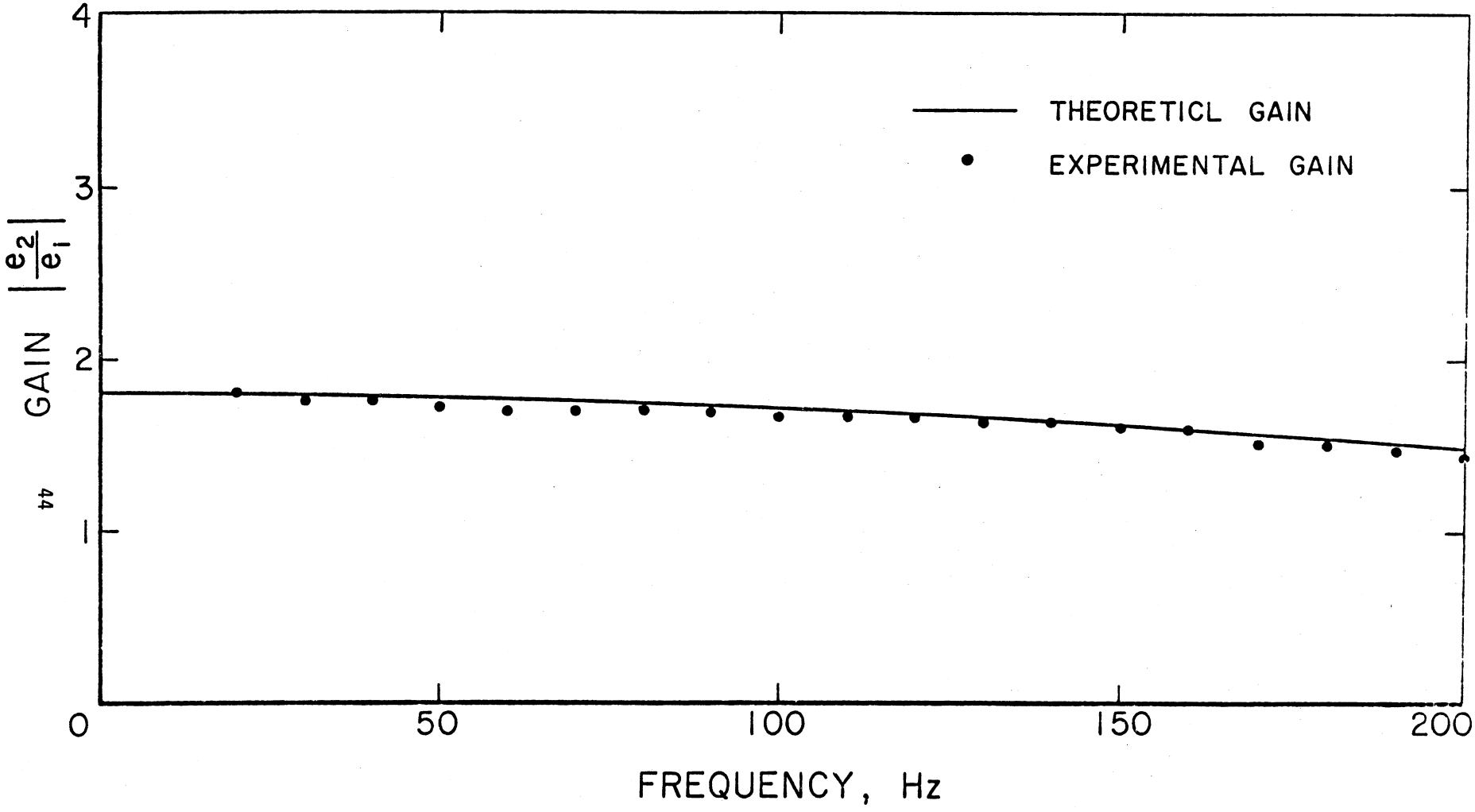

Figure 18. Theoretical and Experimental Gain of $\frac{e_2}{e_i}$ Versus Frequency.

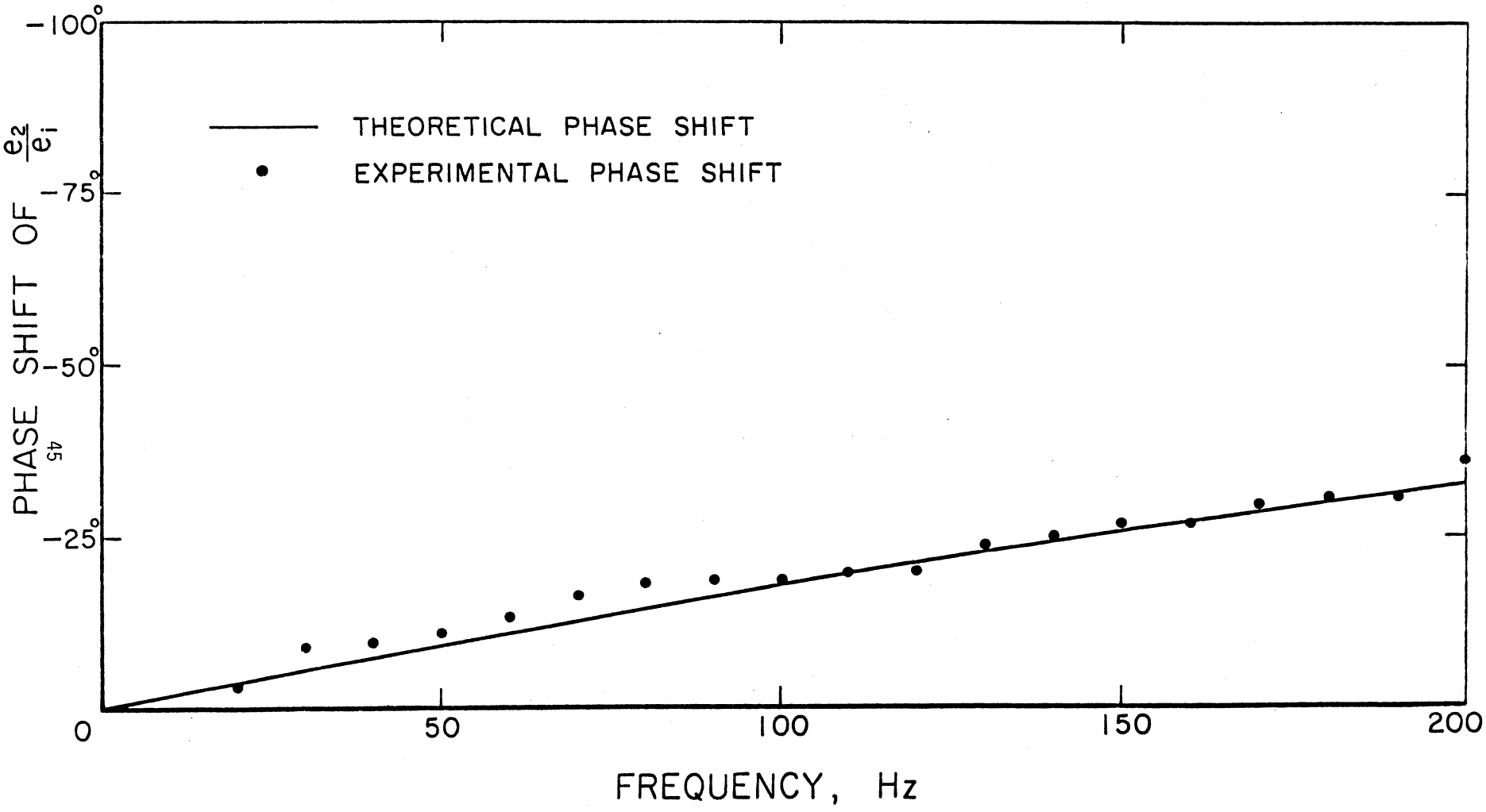

Figure 19. Theoretical and Experimental Phase Shift of $\frac{e_2}{e_i}$ Versus Frequency.

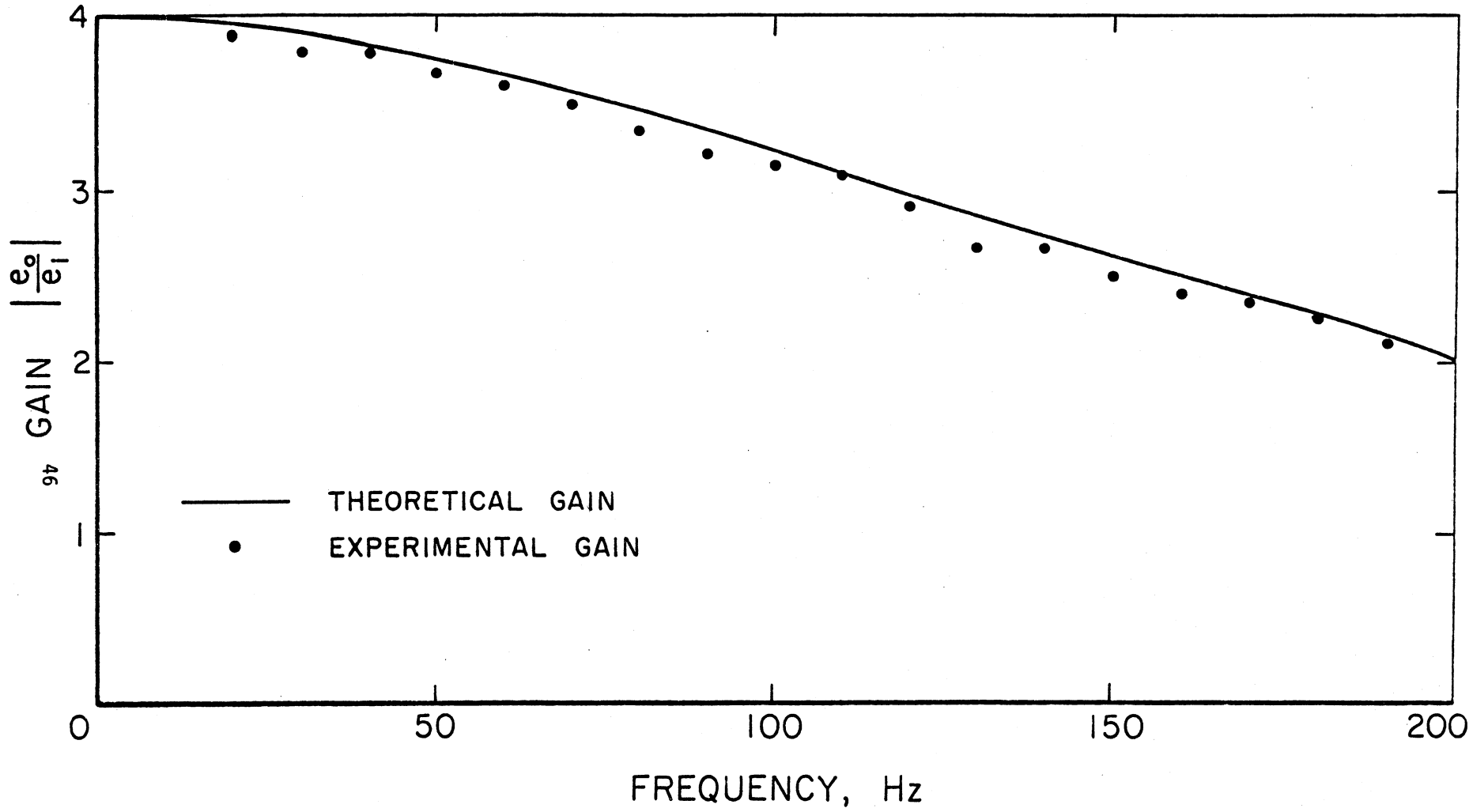

Figure 20. Theoretical and Experimental Gain of $\frac{e_o}{e_i}$ Versus Frequency.

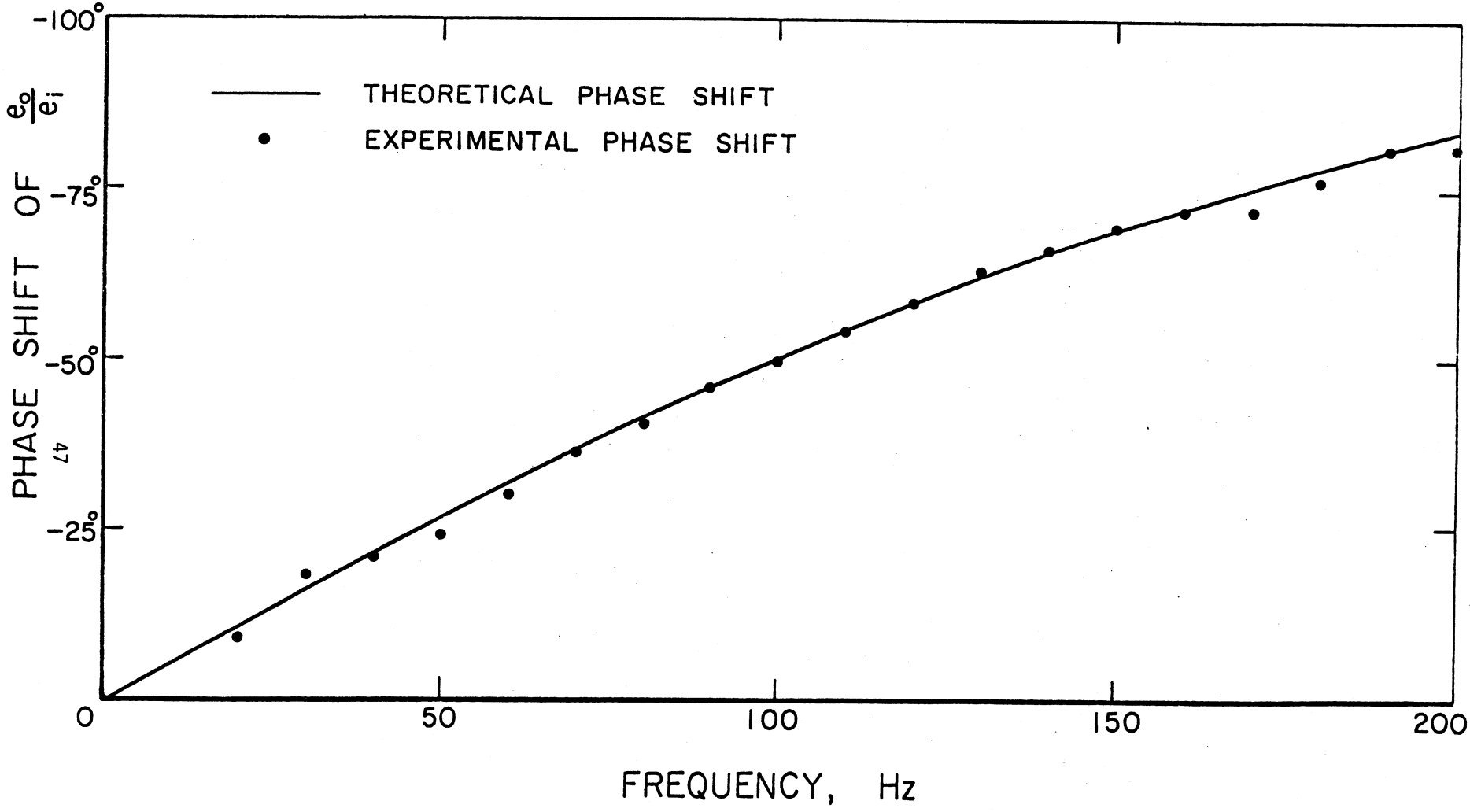

Figure 21. Theoretical and Experimental Phase Shift of $\frac{e_o}{e_i}$ Versus Frequency.

of both filters were neglected. Also, Kinemetrics, Inc., so far did not take these filters into account in their calculations. This assumption is correct as long as very low frequencies are of interest. Neglecting the two filters in the derivation of the final transfer function implies that the system acts as a second-order differential equation [see Equations (48) and (51)]. But as it has been noted at higher frequency the contributions of Parts 1 and 3 to the transfer function are not negligible and must be included in the calculation of the system transfer function and in the use of the differential equation [see Equation (47)]. This produces a fourth-order differential equation instead of Equation (49).

Task 3

This part presents the shaking table test procedure and the results. There are two transducers involved in this test, the Kinemetrics FBA-1 (# 11749), and the Endevco accelerometer (PA80-2272) which was used as the reference accelerometer. The reference accelerometer has a corner frequency of 7,000 Hz and a flat frequency response in the range from 5 Hz to 3000 Hz. The shaking test was performed at Kinemetrics, Inc. The equipment used for this test consisted of the following:

i) SMA-3 control panel to provide a) ± 12 VDC power to the FBA-1 and b) calibration capability.

ii) Tektronix 2215 (dual channel) oscilloscope to monitor the data from the FBA-1 and from the reference accelerometer during the shaking test.

iii) Data from the shaking test were analyzed by Hewlett-Packard 3582A, dual channel spectrum analyzer.

iv) Hewlett-Packard 7015B X-Y plotter was used to plot the transfer function of the FBA-1 with respect to the reference accelerometer.

v) The shaking table used was manufactured by Electro-Seis. (Model 113) of Acoustic Power System, Inc., along with the Power Amplifier Model 114

vi) Hewlett-Packard 3310A Function Generator was used to generate sinusoidal waves.

Other standard laboratory instruments such as a digital voltmeter, frequency meter and a DC power supply were utilzied in this experiment.

Two forms of excitation were utilized in this experiment. The first source was the random noise generator of the HP3582A Spectrum Analyzer. This excitation contained all frequencies in the range of interest (0-100 HZ). The second source was a function generator used to generate sinusoidal waves at discrete frequencies, from 5 HZ to 100 HZ, in the interval of about 5 HZ. In this case the transfer function of the FBA-1 (ratio of the FBA-1 response to the response of the reference accelerometer) was obtained as a discrete set of points.

Figure 22 illustrates the block diagram of the shaking test. The shaker was excited by random noise or sinusoidal wave through the power amplifier. The FBA-1 and the reference accelerometer (Endevco 2272) experienced the same excitation. Data from sensors were monitored using the oscilloscope, and the transfer function of the FBA-1 with respect to the reference accelerometer was obtained from HP3582A Spectrum Analyzer. The evaluation of the transfer function of the FBA-1 is a simple task using the Spectrum Analyzer. It directly computes the transfer function values between two channels of data. A total of 64 linear averages of the 128 spectral estimates

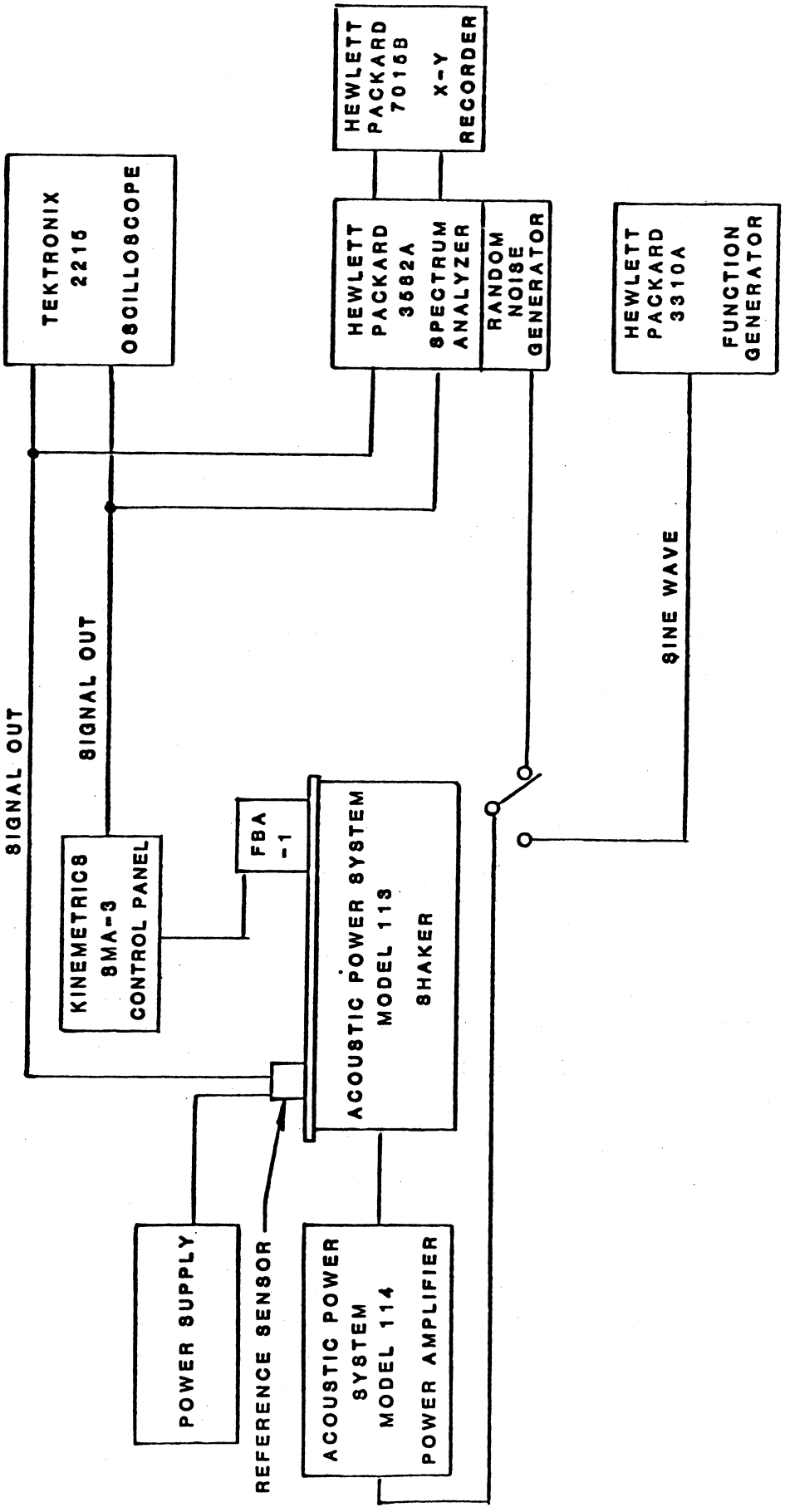

Figure 22. Shaking Table Test Block Diagram.

were used to obtain Signal-to-noise enhancement, and to improve the statistical confidence in the results. The coherence function between FBA-1 and the reference accelerometer was also computed by HP3582A Spectrum Analyzer.

The working assumption is that the ratio of Fourier Transform of the FBA-1 output to that of the reference accelerometer results in the transfer function of the FBA-1. This is because the Endevco 2272 accelerometer has a flat frequencey response in the frequency range from 5 to 3000 Hz. The Frequency range chosen was only from 0 Hz to 100 Hz.

For the case of random noise excitation, the results of the test which were recorded on the HP3582A analyzer were plotted using HP7015B X-Y plotter. For the case of sinusoidal wave excitation, the values of the transfer function of the FBA-1 at different frequencies were recorded from the analyzer and then plotted over the previous results.

The results of this test are shown in Figures 23 and 24. Figure 23 shows the transfer function of the FBA-1 and Figure 24 shows the coherence function between the outputs of FBA-1 and the Endevco 2272. The plot of coherence function between the outputs of two accelerometers indicates good accuracy of the results in the range of 5 to 100 Hz. The shaker frequency response indicated no resonant frequency from 0 to 100 Hz.

The shaking test results indicate a flat transfer function of the FBA-1 in the range from about 0 to 30 Hz before the roll-off occurs. The experimental results are identical for the two sources of excitation. To evaluate the natural frequency and damping from this result the square of the error between the shaking test transfer function result and a single-degree-of-freedom system (Equation 48) were evaluated for different natural frequencies and fractions of critical damping. The minimum error obtained was for values f_n = 43.0 Hz and ζ = 0.61. The theoretical amplitudes for these optimum values

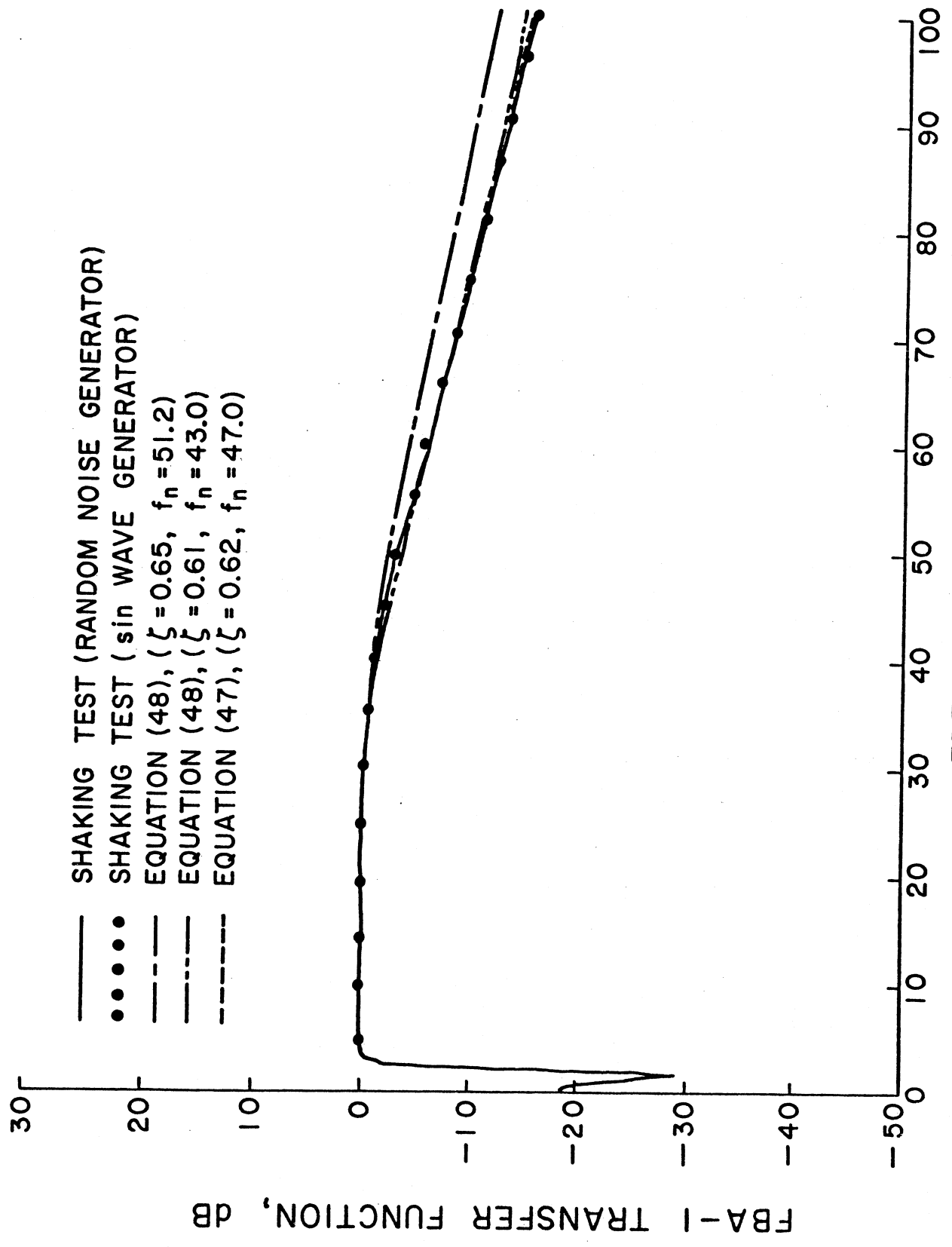

Figure 23. Transfer Function Amplitude of the FBA-1

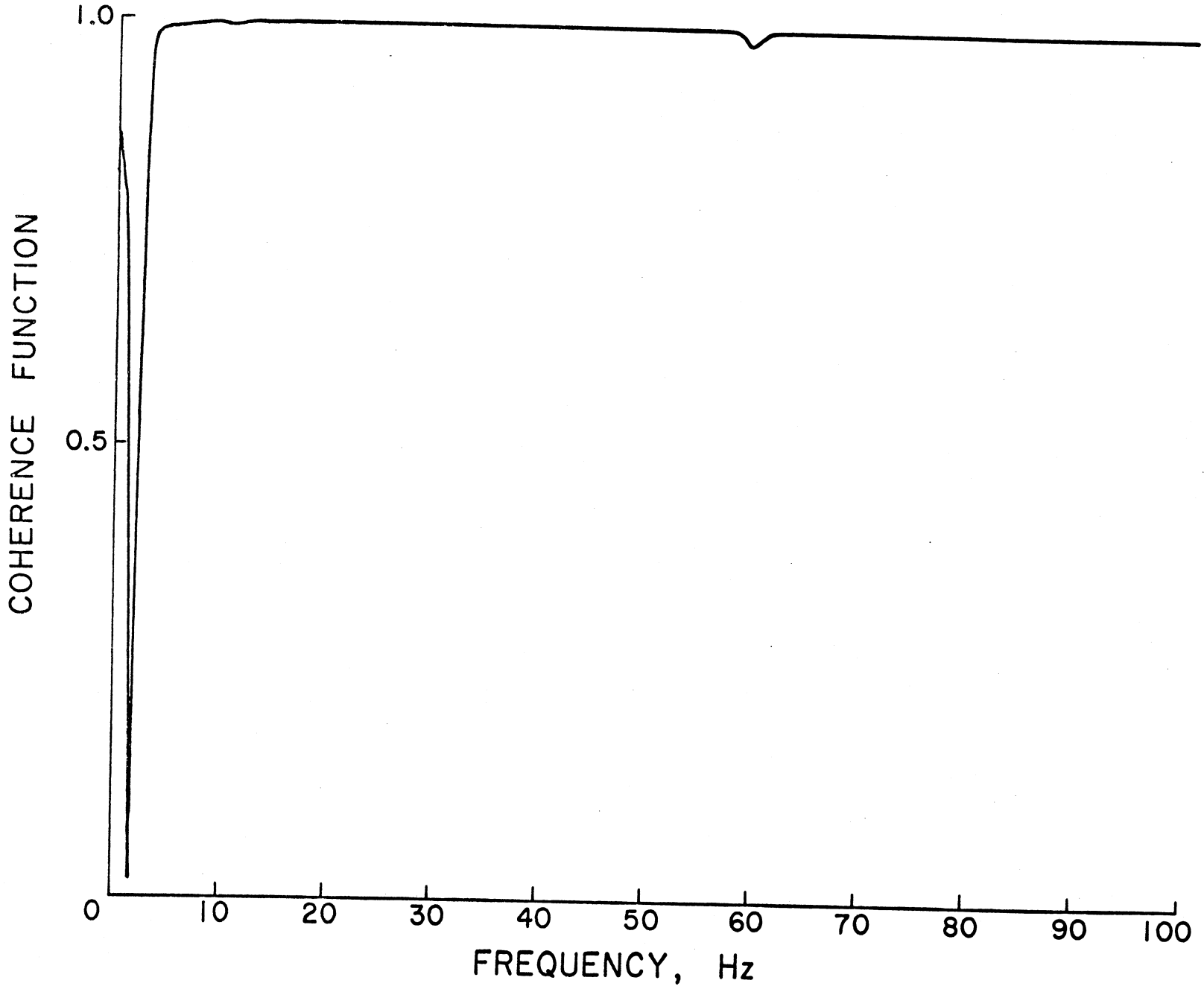

Figure 24. Coherence Function of the FBA-1 with Respect to the Reference Accelerometer (Endevco 2272)

are plotted in Figure 23. Next the square of the difference between the shaking test transfer function result and Equation (47) (disregarding the amplification factors) was also obtained for different natural frequencies and critical damping values. The estimates obtained for this case were f_n = 47.0 Hz and ζ = 0.62. The theoretical response amplitudes corresponding to these optimum values is also shown in Figure 23. The transfer function of the FBA-1, based on Kinemetrics Calibration (Figure 6) and Equation (48) is also shown in Figure 23.

It should be pointed out that the amplitude of the transfer function at f = 0 is not of importance here, since all plots in Figure 23 are of normalized form. The actual gain values have been verified in Figures 18 and 20.

The transfer functions obtained from Equation (47) (f_n = 47.0 Hz, ζ = 0.62) and Equation (48) (f_n = 43.0 Hz, ζ = 0.61) are in very close agreement with the shaking test results. However, due to the presence of the low pass filters in the circuit of the FBA-1, the plot obtained by Equation (47) is more accurate and fits the experimental results better. It is clear that the transfer function of the FBA-1 based on Kinemetrics calibration data (Figure 6) and Equation (48) (ignoring the presence of filters) does not fit the experimental results as well.

Conclusions

Based on the above theoretical and experimental analyses, the following conclusions can be stated.

1. The output of FBA-1 (voltage e_o) is directly proportional to relative displacement X_r only. This produces a response similar to that of conventional transducers (see Figure 15). General results of Hudson (Figure 2) indicate that the output voltage of an FBA can be porportional to a sum of transducer relative displacement and velocity, thus increasing the frequency range before roll-off occurs. Therefore, one possible improvement could be achieved by redesigning the system so that the output voltage includes a velocity contribution, thus producing the response of the form shown in Figures 2 and 3.
2. It was pointed out that because of the variable capacitance a modulation system is required. This modulation uses a carrier sine wave of 17 volts p-p with a frequency of about 10 KHz. However, once the relative displacement is sensed by the variable capacitance, the high-frequency signals must be filtered. The purpose of Parts 1 and 3 is to eliminate the high-frequency signals. But as was seen in Figures 20 and 21, this results in appreciable gain drop and phase shift as frequency increases to 200 Hz. At high frequencies one cannot assume that the system acts as a second-order differential Equation (48), and the contributions of Part 1 and 3 must be included. In other words, Equation (47) must be used. High frequency response could be improved by redesigning filters to have higher corner frequencies thus, decreasing the large gain drop at high values of frequency, or by using a higher frequency (greater than 10 KHz) carrier sine

wave. This would allow the use of filters with higher corner frequencies.

3. Damping and natural frequency are among the most important parameters of any transducer. Due to strong dependence of the response on these parameters, these must be measured accurately. As it was shown in Figure 17 following the original Kinemetrics test procedure, damping and natural frequency were calculated to be 0.67 and 49.73 Hz, respectively. In yet another testing procedure explained above, which was done at Kinemetrics, Inc., the results were 0.65 for damping and 51.2 Hz for natural frequency (see Figure 6).

Shaking table test results of Figure 23 indicate damping and natural frequency of 0.61 and 43.0 Hz respectively when the filters are not considered (Equation 48). However, when the filters are included (Equation 47), damping and natural frequency of 0.62 and 47.0 Hz seem to best fit the shaking test results. The values of 0.62 for the critical damping and 32.0 Hz for natural frequency satisfy Equations (38) and (39) simultaneously. However, it should be clear that Equations (38) and (39) are only the approximations of Equations (32) and (33) respectively.

It is apparent from Equation (39) that the square of the natural frequency is inversely proportional to R_o and directly proportional to R_h (value of R_8 is usually kept constant). Equation (38) indicates that the product of natural frequency and damping is directly proportional to R_h. In fact, this verifies the procedure Kinemetrics, Inc., uses to alter the values of natural frequency and damping. In the FBA Adjustment Procedure, natural frequency is determined by selecting proper resistance for R_o, and damping is adjusted by selecting proper resistance for R_h. The main part of the critical damping is produced by the capacitor C*.

It should also be pointed out that in the first measurement based on operating instructions of FBA-1 for natural frequency (fn = 49.73), resistance R_{12} with a value of 330 ohms (see Figure 4) comes into the circuit which is ordinarily grounded on both sides and has no effect on the transfer function of the system, while FBA-1 is subjected to strong ground acceleration.

In the test done by Kinemetrics for measurements of damping and natural frequency (ζ = 0.65, f_n = 51.2 Hz) another portion of the circuit which includes diode CR_o, 10 K potentiometer, and R_{cal} comes into action which is again normally isolated when FBA-1 is measuring strong ground acceleration. It is believed in both of the above cases a resistance parallel to R_o is introduced, hence reducing the effective value of R_o in the equations derived. This, as a result, increases the value of natural frequency.

It is noted that at frequency of 50 Hz, there is an appreciable gain drop of about 6% (see Figure 20) just due to filters of stages 1 and 3.

References

1. Comer, David J., Introduction to Semiconductor Circuit Design, Addison-Wesley Publishing Co., 1968

2. Clough, Ray W., and Penzien, Joseph, Dynamics of Structures, McGraw-Hill, Inc., 1975.

3. Hudson, D. E. (1979) Unpublished notes and personal communication.

4. Neubert, Herman K., Instrument Transducers: An Introduction to their Performance and Design, Oxford, Clarendon, Press, 1975 (2nd ed.).

5. Norton, Harry N., Handbook of Transducers for Electronic Measuring Systems, Englewood Cliffs, N. J., Prentice Hall, 1969.

6. Ogata, Katsuhiko, Modern Control Engineering, Englewood Cliffs, Prentice Hall, 1970.

7. Oliver, Frank J., Practical Instrumentation Transducers, New York, Hayden Book Co., 1971.

8. Rhin, W. J., "Magnetic Tape Recording and Processing of Strong-Motion Data," Fifth World Conference on Earthquake Engineering, Session 3C: Earthquake Instrumentation, Rome, 1973.

9. Slemon, Gordon R., Magnetoelectric Devices: Transducers, Transformers, and Machines, New York, Wiley, 1966.

10. Smith, Ralph J., Circuits, Devices, and Systems, New York, John Wiley and Sons, Inc., 1971

Acknowledgements

We wish to thank D. E. Hudson for useful discussion and for critical reading of the manuscript. One group of the shaking table experiments was carried out at Kinemetrics, Inc. in Pasadena. The cooperation, help and comments of the Kinemetrics staff is gratefully acknowledged.

This research was supported by a grant from the National Science Foundation.